Cell Metabolism
Article

CB_1 Signaling in Forebrain and Sympathetic Neurons Is a Key Determinant of Endocannabinoid Actions on Energy Balance

Carmelo Quarta,[1,18] Luigi Bellocchio,[2,3,18] Giacomo Mancini,[4,18] Roberta Mazza,[1] Cristina Cervino,[1] Luzie J. Braulke,[6] Csaba Fekete,[7,8] Rocco Latorre,[9] Cristina Nanni,[10] Marco Bucci,[1,11] Laura E. Clemens,[6] Gerhard Heldmaier,[6] Masahiko Watanabe,[12] Thierry Leste-Lassere,[2,3] Marlène Maitre,[2,3] Laura Tedesco,[13,14] Flaminia Fanelli,[1] Stefan Reuss,[5] Susanne Klaus,[15] Raj Kamal Srivastava,[4] Krisztina Monory,[4] Alessandra Valerio,[13,16] Annamaria Grandis,[17] Roberto De Giorgio,[9] Renato Pasquali,[1] Enzo Nisoli,[13,14] Daniela Cota,[2,3] Beat Lutz,[4] Giovanni Marsicano,[2,3] and Uberto Pagotto[1,*]

[1]Endocrinology Unit and Centro di Ricerca Biomedica Applicata, Department of Clinical Medicine, University of Bologna, Bologna 40138, Italy
[2]INSERM U862 Neurocentre Magendie, Bordeaux 33077, France
[3]Université Bordeaux, Bordeaux 33077, France
[4]Institute of Physiological Chemistry
[5]Institute of Anatomy and Cell Biology
University Medical Center of the Johannes Gutenberg University Mainz, Mainz 55099, Germany
[6]Department of Biology Animal Physiology, Philipps University Marburg, Marburg 35032, Germany
[7]Department of Endocrine Neurobiology, Institute of Experimental Medicine, Hungarian Academy of Sciences, Budapest 1083, Hungary
[8]Division of Endocrinology, Diabetes, and Metabolism, Tupper Research Institute and Department of Medicine, Tufts Medical Center, Boston, MA 02111, USA
[9]Department of Clinical Medicine and Centro di Ricerca Biomedica Applicata
[10]Department of Nuclear Medicine, S. Orsola-Malpighi Hospital
University of Bologna, Bologna 40138, Italy
[11]Turku PET Centre, University of Turku, 20521 Turku, Finland
[12]Department of Anatomy, Hokkaido University School of Medicine, Sapporo 060-8638, Japan
[13]Integrated Laboratories Network, Center for Study and Research on Obesity, Department of Pharmacology, Chemotherapy, and Medical Toxicology, Università degli Studi di Milano, Milano 20129, Italy
[14]Istituto Auxologico Italiano, Milano 20145, Italy
[15]Department of Pharmacology, German Institute of Human Nutrition Potsdam-Rehbruecke, Nuthetal 14558, Germany
[16]Department of Biomedical Sciences and Biotechnologies, University of Brescia, Brescia 25123, Italy
[17]Department of Veterinary Morphophysiology and Animal Productions, University of Bologna, 40064 Ozzano dell'Emilia, Bologna 40138, Italy
[18]These authors contributed equally to this work
*Correspondence: uberto.pagotto@unibo.it
DOI 10.1016/j.cmet.2010.02.015

SUMMARY

The endocannabinoid system (ECS) plays a critical role in obesity development. The pharmacological blockade of cannabinoid receptor type 1 (CB_1) has been shown to reduce body weight and to alleviate obesity-related metabolic disorders. An unsolved question is at which anatomical level CB_1 modulates energy balance and the mechanisms involved in its action. Here, we demonstrate that CB_1 receptors expressed in forebrain and sympathetic neurons play a key role in the pathophysiological development of diet-induced obesity. Conditional mutant mice lacking CB_1 expression in neurons known to control energy balance, but not in nonneuronal peripheral organs, displayed a lean phenotype and resistance to diet-induced obesity. This phenotype results from an increase in lipid oxidation and thermogenesis as a consequence of an enhanced sympathetic tone and a decrease in energy absorption. In conclusion, CB_1 signaling in the forebrain and sympathetic neurons is a key determinant of the ECS control of energy balance.

INTRODUCTION

The endocannabinoid system (ECS) has emerged as a key player in both central and peripheral functions related to energy metabolism (Pagotto et al., 2006; Kunos et al., 2008). Initial studies based on the evidence that the cannabinoid receptor type 1 (CB_1) was exclusively present in the brain all attributed the ability of the ECS to modulate food intake to a central site of action (Pagotto et al., 2006). However, new evidence has accumulated, which suggests that the ECS might regulate energy balance not exclusively at central sites. In fact, CB_1 receptors and their ligands were also found in several peripheral organs (Pagotto et al., 2006; Kunos et al., 2008). Consequently, it has emerged that CB_1 might control body weight by food intake-independent mechanisms. Complete deletion of CB_1 in mice (CB_1-KO) led to decreased fat mass, reduced body weight, and resistance to develop obesity (Cota et al., 2003; Ravinet Trillou et al., 2004). In addition, beneficial food intake-independent effects on metabolism were demonstrated by using CB_1 antagonists

(Ravinet Trillou et al., 2004). Recent studies suggested that the sustained body weight loss induced by CB_1 antagonists after the initial decrease in food intake might be explained by an effect of the drugs on energy expenditure. Blockade of CB_1 in obese animals induces an array of pharmacological effects, including stimulation of lipolysis and fatty acid oxidation (Herling et al., 2008). However, the anatomical location of the CB_1 receptors involved in these functions is still under discussion (Kunos et al., 2009). This is an important point because rimonabant, the first CB_1 antagonist used for the treatment of obesity, has been recently withdrawn from the market due to psychiatric side effects (Akbas et al., 2009). The generation of CB_1 antagonists selectively acting at peripheral organs could be a promising way to preserve the metabolic effects of CB_1 blockade without causing side effects due to CB_1 inhibition in neural circuits regulating mood and anxiety (McElroy et al., 2008; LoVerme et al., 2009). Nevertheless, the identification of the anatomical site(s) where the ECS exerts its effects on energy balance and metabolism is mandatory before further screening for potentially more selective and safer drugs. Thus, in order to single out the major anatomical sites underlying the ECS-dependent regulation of energy balance and metabolism, we studied conditional mutant mice (CaMK-*CB_1*-KO mice) characterized by a CB_1 deletion in forebrain neurons (Marsicano et al., 2003) and compared their phenotype to that of conventional *CB_1*-KO (Marsicano et al., 2002) and of mice treated with the CB_1 antagonist rimonabant.

RESULTS

Anatomical Characterization of CB_1 Expression in CaMK-*CB_1*-KO Mice

CaMK-*CB_1*-KO conditional mutant mice were obtained using the Cre/loxP system by crossing *CB_1*$^{flox/flox}$ mutants with CaMKIIα-iCre transgenic mice (Casanova et al., 2001; Marsicano et al., 2003). CaMKIIα-iCre mice express the recombinase in the great majority of adult forebrain neurons, with the exclusion of cortical GABAergic interneurons (Casanova et al., 2001). Importantly, brain regions known to control energy balance (e.g., the hypothalamus) do express the Cre recombinase in these mutant mice (Casanova et al., 2001).

As expected, the abundant expression of CB_1 mRNA in intrinsic neurons of the hypothalamus (Cota et al., 2003) (Figures 1A and 1B) was absent in CaMK-*CB_1*-KO mice (Figures 1A and 1B). In the hypothalamus, CB_1 protein was found mainly on axon terminals of both extrinsic and intrinsic neurons (Wittmann et al., 2007). Immunohistochemistry (IHC) revealed that the intensely CB_1-positive meshwork in the hypothalamus of CaMK-*CB_1*-WT was virtually absent in CaMK-*CB_1*-KO mice (Figures 1A and 1B).

The nucleus of the solitary tract (NTS) is one of the main funneling sites of energy balance regulation (Grill and Hayes, 2009). It receives inputs from both higher brain regions (as hypothalamus and cerebral cortex) and vagal ganglions (i.e., nodose ganglion) and regulates output efferents that control the functions of several peripheral organs modulating energy metabolism (Grill and Hayes, 2009). Similar to the hypothalamus, CB_1 receptors are present in both afferent and efferent neurons of the NTS (Tsou et al., 1998). Intrinsic NTS neurons of CaMK-*CB_1*-KO mice still expressed CB_1 mRNA, as revealed by double in situ hybridization (DISH) using glucagon-like peptide 1, a marker of NTS neurons (Figure 1C). However, no CB_1 protein was found in this region (Figure 1C). Thus, these data indicate that the afferent terminals in the NTS of CaMK-*CB_1*-KO mice do not contain CB_1 protein. Because CB_1 protein is expressed generally at presynaptic level, the preserved CB_1 mRNA expression in intrinsic NTS neurons suggests that CB_1 protein at the axonal terminals of these neurons is present in mutant mice. CB_1 mRNA expression is preserved in both rostral and distal nodose ganglion (Figures 1D and 1F and Figure S1A available online) of CaMK-*CB_1*-KO, and CB_1 immunoreactivity is also unchanged in these mutant mice as compared to WT (Figure S1B). Thus, CB_1 signaling on vagal afferents to NTS and to the nodose ganglion is maintained in CaMK-*CB_1*-KO mice. CB_1 mRNA is also present in a subset of dopamine-β-hydroxylase (DBH)-expressing neurons of superior cervical sympathetic ganglia but is significantly reduced as compared to WT (Figure 1E). The neuroanatomical analysis was in agreement with QT-PCR data showing a nearly 60% reduction in the ratio between CB_1 and DBH mRNA expression in superior cervical ganglia of CaMK-*CB_1*-KO mice (data not shown). Conversely, CB_1 expression was preserved in nonneuronal peripheral organs (Figures 1F and 1G).

CaMK-*CB_1*-KO Mice Are Lean and Unresponsive to the Acute Action of the CB_1 Antagonist Rimonabant

The monitoring of body weight in mice maintained on standard diet (SD) revealed that CaMK-*CB_1*-KO mice had a significantly lower body weight than their WT (Figure 2A). However, when compared to complete *CB_1*-KO mice, the phenotype of conditional mutants was less pronounced (Figures 2B and 2C), suggesting that CB_1 expressed in forebrain and sympathetic neurons does not fully account for the lean phenotype observed in the complete *CB_1*-KO mice on SD.

The CB_1 antagonist rimonabant exerts profound CB_1-dependent effects on food intake, body weight, and lipid oxidation (Herling et al., 2008). To investigate whether these effects are dependent upon CB_1 in forebrain and sympathetic neurons, CaMK-*CB_1*-KO and WT littermates were treated with rimonabant. The administration of the CB_1 antagonist acutely reduced body weight and respiratory quotient (RQ) of CaMK-*CB_1*-WT mice, but not of CaMK-*CB_1*-KO mice (Figures 2D and 2E). Furthermore, because the effects of acute CB_1 blockade are particularly evident in stimulated conditions (Di Marzo et al., 2001), we evaluated rimonabant action on fasting-induced overeating in conditional mutant mice. After 24 hr of fasting, CaMK-*CB_1*-WT mice ate significantly more than CaMK-*CB_1*-KO mice (Figure 2F). Under these experimental conditions, rimonabant (3 mg/kg i.p.) significantly decreased food intake in CaMK-*CB_1*-WT, unlike in CaMK-*CB_1*-KO (Figure 2F). These data indicate that CB_1 expressed in forebrain and sympathetic neurons is an important mediator of the acute effects of rimonabant on food intake, body weight, and lipid oxidation.

CB_1 in Forebrain and Sympathetic Neurons Regulates Diet-Induced Obesity

To assess the role of CB_1 in diet-induced obesity (DIO), CaMK-*CB_1*-KO, complete *CB_1*-KO, and their WT littermates were maintained on a mild high-fat diet (HFD, 40% fat content) for 12 weeks.

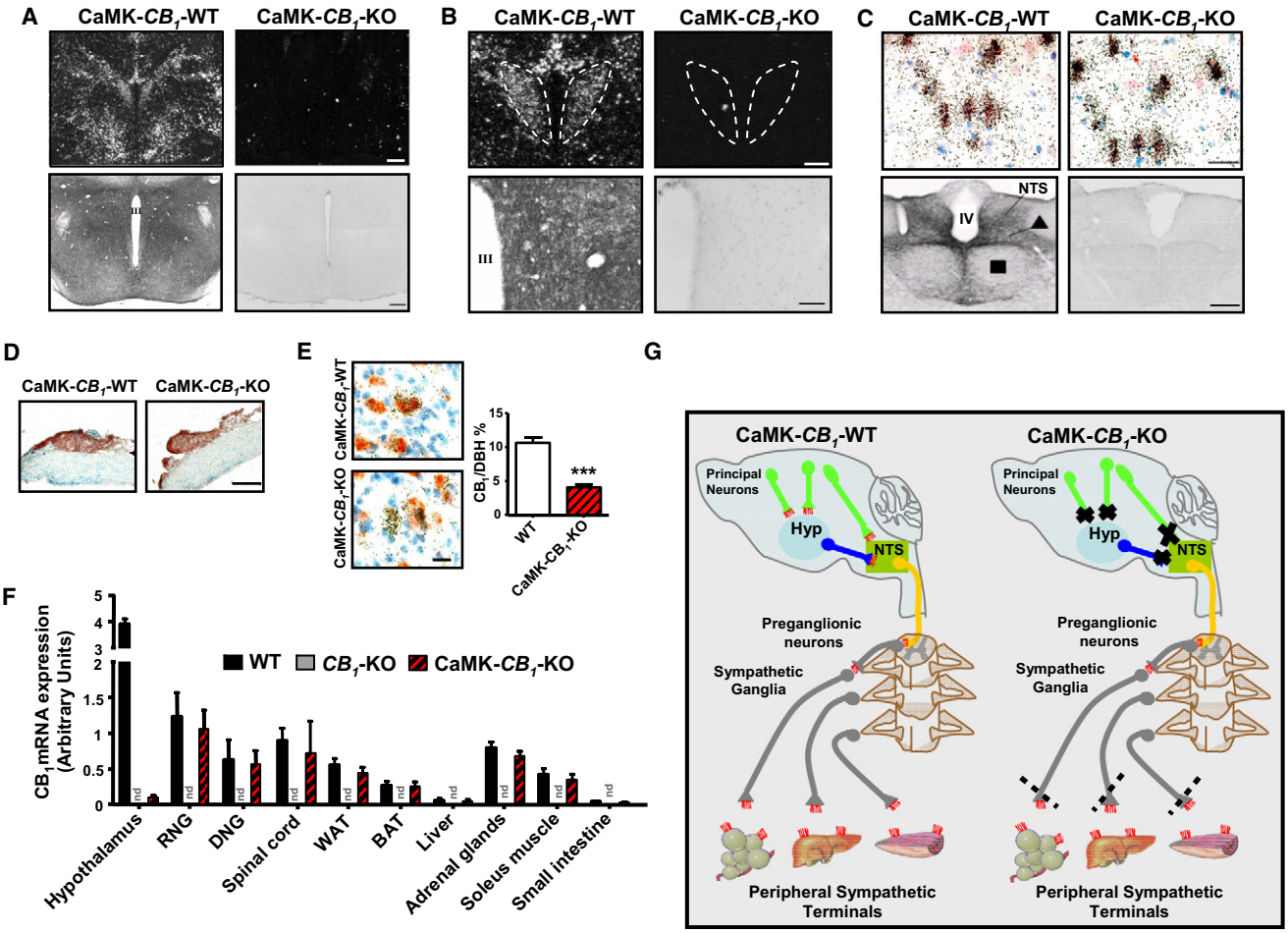

Figure 1. CB_1 mRNA and Protein Distribution in CaMK-CB_1-KO Mice

(A) CB_1 mRNA expression detected by ISH (top) and staining of CB_1 protein by IHC (bottom) in the whole hypothalamus. Scale bar, 200 μm.

(B) ISH (top) and IHC (bottom) for CB_1 in the paraventricular nucleus of the hypothalamus (PVN, encircled scattered lines in top panels). Scale bar, 50 μm. (III) third ventricle.

(C) (Top) DISH for CB_1 mRNA (black dots) and glucagon-like peptide 1 (GLP-1) mRNA (red color) in the nucleus of the solitary tract (NTS). Scale bar, 30 μm. (Bottom) CB_1 protein in the NTS. (Triangle) Dorsal motor nucleus of the vagus. (Square) Hypoglossal nucleus. (IV) Fourth ventricle. Scale bar, 200 μm.

(D) ISH for CB_1 mRNA (in red) in the nodose ganglia. Scale bar, 50 μm.

(E) DISH for CB_1 mRNA (black dots) and dopamine-β-hydroxylase (DBH) (red color) and QT-PCR analysis of the ratio CB_1/DBH mRNA expression in the superior cervical sympathetic ganglia. Scale bar, 1.5 μm; n = 4 ganglia per group; data are mean ± SEM. ***$p \leq 0.0005$.

(F) CB_1 mRNA expression by QT-PCR in the hypothalamus and in peripheral tissues of CaMK-CB_1-WT and KO mice (n = 6 per genotype). CB_1-KO mice organs are negative control. WAT, white adipose tissue; BAT, brown adipose tissue, RNG, rostral nodose ganglion; DNG, distal nodose ganglion; n.d., not detected. Data are mean ± SEM.

(G) Schematic representation of areas of CB_1 deletion in CaMK-CB_1-KO mice, referring to regions implicated in energy control. Presynaptic CB_1 protein is in red. Black crosses indicate CB_1 deletion. Dashed lines indicate reduced CB_1 expression. Hyp, hypothalamus; NTS, nucleus of the solitary tract.

See also Figure S1.

To study CB_1 expression in peripheral tissues after HFD, we analyzed, by QT-PCR, CB_1 mRNA levels in white adipose tissue (WAT), brown adipose tissue (BAT), and liver of CaMK-CB_1-KO and -WT. QT-PCR analysis in BAT and liver of CaMK-CB_1-WT mice revealed that CB_1 mRNA expression was increased in HFD, as compared to SD (Figure 3A). This increase remained significant only in the liver, but not in the BAT, of CaMK-CB_1-KO. No differences were detected in WAT of both CaMK-CB_1-KO and -WT mice on HFD compared to SD (Figure 3A).

Both CaMK-CB_1-KO and complete CB_1-KO mice had a significantly lower body weight than their WT under HFD (Figures 3B and 3C). However, when body weight was expressed as percentage of the initial weight, CaMK-CB_1-KO mice gained significantly less weight than WT or CB_1-KO mice (Figure 3D). Of interest, the weight gain of complete CB_1-KO was not different from WT. Furthermore, a chronic treatment with rimonabant (10 mg/kg; 32 days, daily) did not affect the body weight of CaMK-CB_1-KO mice under HFD, whereas it reduced body weight gain in CaMK-CB_1-WT (Figure 3E). A diet higher in fat content (60%, super HFD) caused a greater body weight gain in WT mice, but not in CaMK-CB_1-KO mice (Figures 3F and 3G). Thus, these data exclude that the resistant phenotype

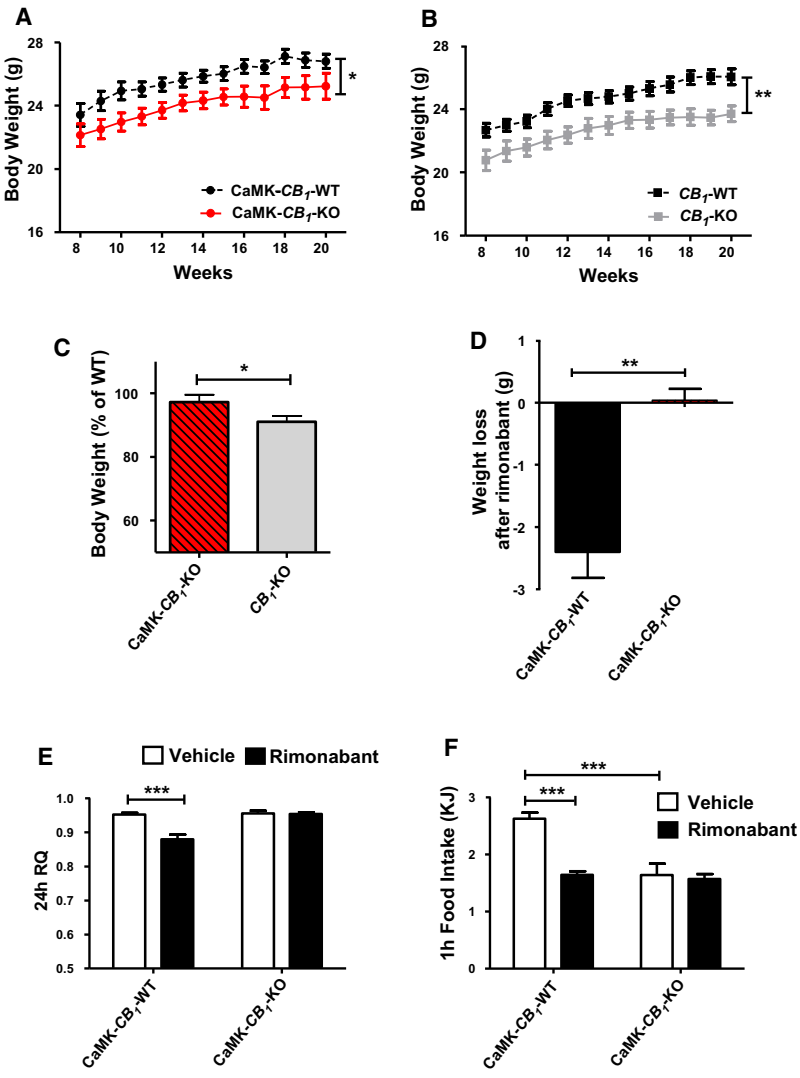

Figure 2. Characterization of CaMK-CB_1-KO Mice during Standard Diet

(A) Average body weight of CaMK-CB_1-WT (black circles) and CaMK-CB_1-KO mice (red circles) kept on SD for a period of 12 weeks (n = 18 per genotype). *p < 0.05.

(B) Average body weight of CB_1-WT mice (black circles) and complete CB_1-KO mice (gray circles) kept on SD for a period of 12 weeks (n = 18 per genotype). **p < 0.005.

(C) Body weight of CaMK-CB_1-KO and complete CB_1-KO mice, expressed as percentage of WT mice ± SEM. Values for CaMK-CB_1-WT and CB_1-WT were cumulated since not statistically different (black bar). Red dashed bar, CaMK-CB_1-KO; gray bar, CB_1-KO mice. *p < 0.05.

(D) Weight loss of CaMK-CB_1-WT mice (black bar) (n = 6) and CaMK-CB_1-KO (red dashed bar) (n = 5) 24 hr after rimonabant administration (10 mg/kg i.p.). **p < 0.005.

(E) Average 24 hr respiratory quotient (RQ) measured every hour for two days in CaMK-CB_1-WT mice (n = 7) and CaMK-CB_1-KO (n = 6). On the first day, animals were treated with vehicle; rimonabant treatment (10 mg/kg i.p.) started at the beginning of day 2. ***p < 0.0005. White bars, vehicle mice; black bars, rimonabant mice.

(F) Cumulative food intake within 1 hr after fasting of CaMK-CB_1-WT mice (black bars) and CaMK-CB_1-KO mice (white bars) treated with vehicle or rimonabant (3 mg/kg i.p.), respectively. n = 10 per genotype. ***p < 0.0005.

Data represent mean ± SEM.

observed in CaMK-CB_1-KO mice was displayed only under conditions of moderate DIO. Furthermore, we measured the total adiposity, hepatic steatosis (by hepatic triglyceride measurement), and plasma metabolic profile of CaMK-CB_1-KO, CB_1-KO, and their respective WT mice after 12 weeks of HFD. No significant difference was observed between WT littermates of CaMK-CB_1-KO mice and CB_1-KO mice, neither under SD nor under HFD (data not shown). Thus, WT values were cumulated to improve readability of the results. As shown in Figures 4A and 4B, chronic HFD did not significantly increase adipose tissue content in CaMK-CB_1-KO and CB_1-KO mice, as opposed to WT. Hepatic triglycerides content was significantly increased in WT animals after HFD administration, but not in CB_1-KO and CaMK-CB_1-KO mice (Figure 4C). The plasma levels of leptin, insulin, glucose, free fatty acids (FFA), and triglycerides were significantly increased in WT animals, but not in CB_1-KO and CaMK-CB_1-KO mice, after the same HFD (Figure 4D). Total cholesterol increased in WT animals after HFD, but no significant changes were observed in either CB_1-KO or CaMK-CB_1-KO mice (Figure 4D). Altogether, these results suggest that CB_1 signaling in forebrain and sympathetic neurons plays an important role in body weight gain, fat accumulation, and metabolic alterations associated with chronic HFD consumption.

Metabolized Energy and Lipids Utilization under HFD Are Modulated by CB_1 in Forebrain and Sympathetic Neurons

CaMK-CB_1-KO and CB_1-KO mice under HFD showed a total food intake comparable to their WT controls (Figures 5A and 5B). Nevertheless, CaMK-CB_1-KO mice had a significantly lower feed efficiency than either WT or complete CB_1-KO mice (Figure 5C). Thus, CB_1 in forebrain and sympathetic neurons regulates the conversion of energy intake into fat accumulation and body weight gain. To analyze the mechanisms underlying the reduced feed efficiency of CaMK-CB_1-KO mice, we evaluated energy homeostasis. First, as compared to their WT littermates, CaMK-CB_1-KO mice exhibited a less-efficient absorption of energy, as indicated by the increase in the energy content of the feces (Figure 5D). CaMK-CB_1-KO mice and their WT littermates had comparable metabolic rate (Figure 5E) and body temperature (data not shown). Conversely, the RQ was significantly reduced in the mutant animals during the night, the active period of mice (Figure 5F). No difference in night and day food intake was found between CaMK-CB_1-KO and CaMK-CB_1-WT mice (data not shown), thus allowing us to exclude that a different amount of food ingested in the dark period influenced the RQ. As in SD (Figure 2E), the acute administration of rimonabant in HFD reduced RQ in CaMK-CB_1-WT mice, but not in CaMK-CB_1-KO mice (Figure 5G).

CB_1 in Forebrain and Sympathetic Neurons Regulates BAT Functions and Thermogenesis

Low feed efficiency may be also explained by increased BAT thermogenic and mitochondrial activities. Of note, peroxisome proliferator-activated receptor γ coactivator 1α (PGC-1α), nuclear respiratory factor-1 (NRF-1), mitochondrial transcription factor A (Tfam) (master regulators of mitochondrial biogenesis), and cytochrome c (Cyt c) and cytochrome c oxidase IV (COX IV) (two mitochondrial proteins involved in oxidative phosphorylation) mRNA levels, as well as mitochondrial DNA amount and citrate synthase activity (biomarkers of mitochondrial mass and function), were significantly increased in BAT of CaMK-*CB_1*-KO as compared to WT (Figure 6A). Western blot analysis confirmed the QT-PCR data. In fact, an increase in PGC-1α, COX IV, and Cyt c protein levels in the BAT of CaMK-*CB_1*-KO mice, as compared to WT mice, was observed (Figure S2A). Furthermore, mRNA levels of uncoupling protein 1 (UCP-1) were significantly increased in BAT of CaMK-*CB_1*-KO mice, as compared to WT mice (Figure 6A), suggesting an increased thermogenic capacity in the conditional mutant mice. To test this hypothesis, we exposed HFD-fed CaMK-*CB_1*-KO mice to a thermal challenge. Body temperature and O_2 consumption were significantly higher in CaMK-*CB_1*-KO mice than in CaMK-*CB_1*-WT mice after cold exposure (+6°C) (Figures 6B and 6C), thus suggesting that the lack of CB_1 in the forebrain neurons improves the thermogenic responses and increases energy expenditure. In vivo positron emission tomography (PET) analysis revealed that the uptake of 2-deoxy-2-[^{18}F]fluoro-D-glucose (^{18}F-FDG) was markedly increased in cold-exposed HFD-fed CaMK-*CB_1*-KO mice, as compared to CaMK-*CB_1*-WT mice (Figures 6D and 6E). Moreover, rimonabant treatment increased the ^{18}F-FDG uptake in CaMK-*CB_1*-WT mice, but not in CaMK-*CB_1*-KO mice (Figure 6E). These data strongly suggest that the activation of neuronal CB_1 signaling modulates BAT thermogenesis during HFD and that CB_1 in forebrain and sympathetic neurons has a major role in the regulation of this function.

CB_1 in Forebrain and Sympathetic Neurons Regulates Energy Balance by Modulating the Sympathetic Tone

To determine the mechanism leading to the energy balance changes observed in CaMK-*CB_1*-KO mice under HFD, we investigated the activity of the sympathetic nervous system (SNS). HFD-fed CaMK-*CB_1*-KO mice had a marked increase in plasma norepinephrine (NE) levels, as compared to WT (no changes in plasma epinephrine and dopamine; data not shown), and similar data were obtained in complete *CB_1*-KO mice (Figure 6F). To further substantiate whether the changes in BAT metabolism were due to increased SNS activity, we investigated the uptake of the PET tracer ^{11}C-meta-hydroxyephedrine (a NE analog) (Thackeray et al., 2007) into the BAT of WT, CaMK-*CB_1*-KO, and *CB_1*-KO mice. Similar increases in tracer uptake were observed in both CaMK-*CB_1*-KO and *CB_1*-KO mice as compared to WT at 24°C, suggesting an increased NE turnover in this tissue (Figure 6G). Consistently, WT mice chronically treated with rimonabant exhibited an increase in BAT NE turnover, as compared to vehicle-treated WT mice (Figure 6H). Moreover, a greater difference in tracer uptake was observed in both conditional and complete KO mice, as compared to WT, under hypothermia (+6°C) (Figure 6G). Altogether, these data suggest that the increased thermogenesis of CaMK-*CB_1*-KO mice is caused by an increased SNS activity in the BAT, implying that CB_1 receptors located in principal forebrain and sympathetic neurons play a key regulator role on peripheral SNS activity. This finding was further substantiated by the in vivo analysis of FDG uptake and ex vivo analysis of mitochondrial activity in the BAT of cold-exposed (+6°C) animals after sympathetic denervation. In vivo small animal PET data demonstrated that the higher thermogenic function of the BAT of CaMK-*CB_1*-KO mice is completely abolished after both chemical (6-OH-dopamine, 6-OH-DA) and surgical sympathectomy (Figure 6E). Moreover, the increase in BAT thermogenesis caused by rimonabant administration is also completely lost after sympathectomy (Figure 6E). Ex vivo analysis of mitochondrial activity in cold-exposed animals after chemical sympathectomy was in agreement with PET data showing that the improved mitochondrial and thermogenic functions of the BAT of CaMK-*CB_1*-KO were lost after sympathectomy (Figure S2B). Altogether, these results demonstrate that an increased NE-mediated sympathetic tone is responsible for the higher thermogenesis in CaMK-*CB_1*-KO mice.

DISCUSSION

This study demonstrates that CB_1 receptors expressed in forebrain and sympathetic neurons play a pivotal role in the regulation of energy balance, which is particularly evident in DIO. Several results support this conclusion: (1) Systemic administration of rimonabant, which antagonizes both neuronal and non-neuronal CB_1, does not affect body weight, food intake, and energy control in CaMK-*CB_1*-KO mice, both under SD or HFD; (2) Whereas CaMK-*CB_1*-KO mice show a milder lean phenotype than *CB_1*-KO mice under SD, their metabolic profile and fat content become indistinguishable after prolonged exposure to HFD; and (3) CaMK-*CB_1*-KO mice are resistant to DIO because of increased thermogenesis and overactivity of the SNS.

The anatomical characterization of CB_1 expression in CaMK-*CB_1*-KO mice demonstrates that this animal model lacks CB_1 protein in glutamatergic forebrain-projecting neurons in the hypothalamus and in the NTS while still preserving the receptor on distal terminals of NTS neurons and on peripheral organs. However, CaMK-*CB_1*-KO mice have a partial deletion of CB_1 in the sympathetic ganglia. Thus, the observed phenotype is the result of the reduced ECS signaling at the level of CB_1 expressed in the forebrain and/or sympathetic neurons.

Our data also show that CB_1 receptors in these locations exert an important role in the control of the metabolic plasmatic profile and hepatic steatosis in DIO. However, this could be secondarily related to the resistance to body weight gain of CaMK-*CB_1*-KO mice and not due to a direct control by CB_1 receptors expressed at these sites. For this reason, our data do not rule out that peripheral CB_1 blockade could directly improve peripheral metabolism, as recently demonstrated (Nogueiras et al., 2008; Osei-Hyiaman et al., 2008; Cota et al., 2009).

Of interest, the overall food intake of conditional mutant mice in HFD is similar to that of WT controls, suggesting that CB_1 receptors control energy balance by other mechanisms than food intake. Indeed, our data show that reduced CB_1 signaling at forebrain and sympathetic neurons counteracts the weight

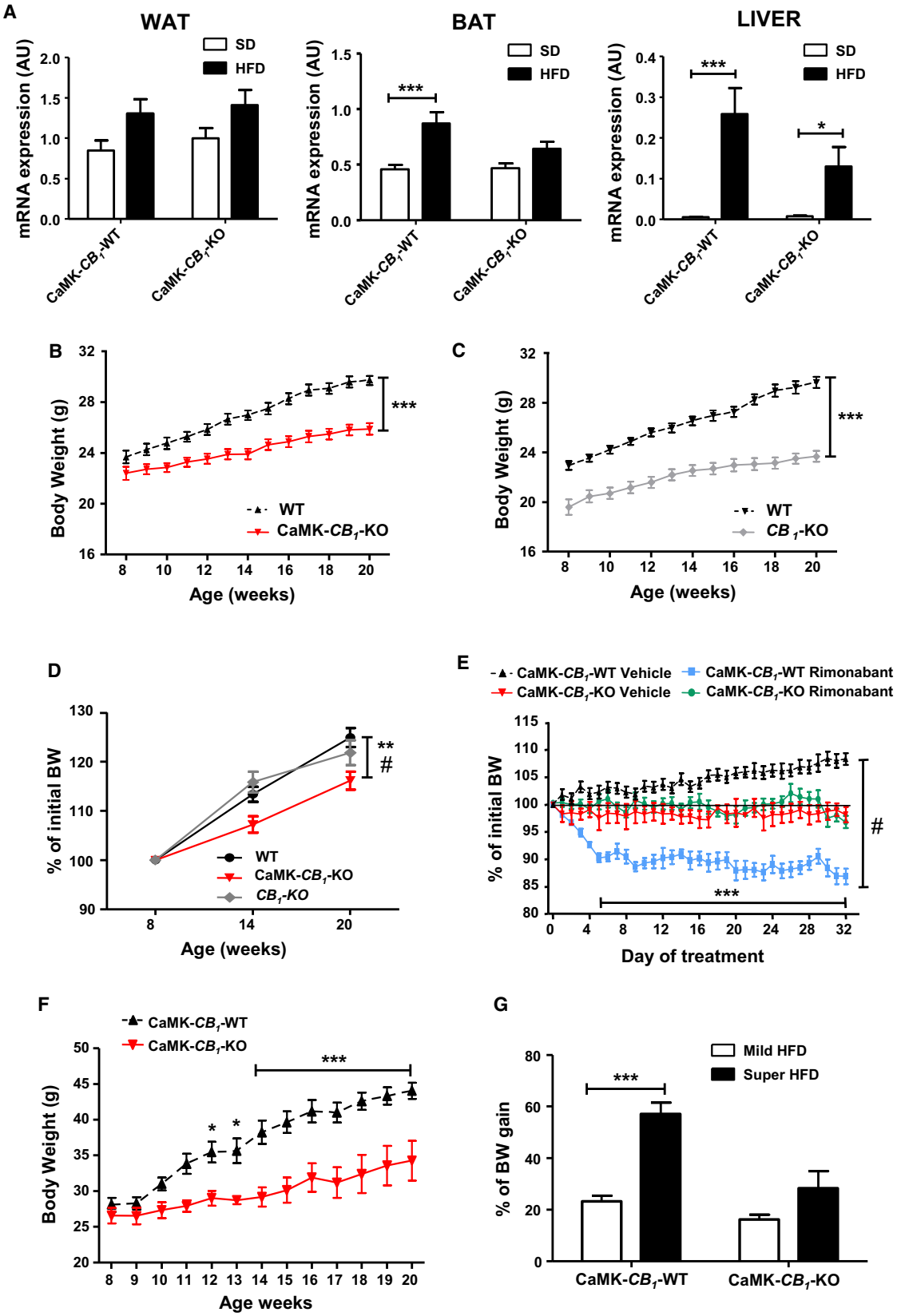
A
WAT
BAT
LIVER
SD
HFD
mRNA expression (AU)
CaMK-CB1-WT
CaMK-CB1-KO
***
*
B
Body Weight (g)
Age (weeks)
WT
CaMK-CB1-KO
C
CB1-KO
D
% of initial BW
**
#
CB1-KO
E
CaMK-CB1-WT Vehicle
CaMK-CB1-KO Vehicle
CaMK-CB1-WT Rimonabant
CaMK-CB1-KO Rimonabant
Day of treatment
F
Age weeks
G
% of BW gain
Mild HFD
Super HFD

gain associated to HFD due to a reduction of metabolized energy and stimulation of lipid oxidation. Thus, blockade of CB_1 signaling at these sites is necessary to induce lipid oxidation, a phenomenon observed during chronic treatment with CB_1 antagonists (Herling et al., 2008).

Furthermore, CaMK-*CB_1*-KO mice display upregulated mitochondrial biogenesis and enhanced thermogenic activity in the BAT. These data are in agreement with previous studies demonstrating that CB_1 blockade promotes energy dissipation through mitochondrial heat production in the BAT, activation of futile cycles, and restoration of mitochondrial biogenesis in WAT of HFD-fed mice (Jbilo et al., 2005; Tedesco et al., 2008). Of note, the increased fatty acid oxidation and the elevation of several indexes of cellular energy dissipation seem to account for the lower feed efficiency observed in CaMK-*CB_1*-KO mice. Thus, the present findings suggest that CB_1 receptors on forebrain and sympathetic neurons play a necessary role in the ECS modulation of energy balance.

Our data demonstrate that CB_1 receptors regulate energy balance by modulating the SNS. Indeed, we found an elevated sympathetic noradrenergic tone in CaMK-*CB_1*-KO mice and an increased NE turnover in the BAT of CaMK-*CB_1*-KO mice, suggesting that enhanced SNS activity is the factor responsible for the increased functional activity of the BAT in CaMK-*CB_1*-KO mice. This conclusion is substantiated by two observations: (1) During acute exposure to cold, a condition stimulating thermogenesis via SNS activation, CaMK-*CB_1*-KO displayed a higher NE turnover of BAT and increased BAT functional activity, and they preserved their metabolic rate and body temperature; and (2) The increased BAT functional activity is lost in CaMK-*CB_1*-KO mice after both chemical and surgical sympathectomy.

The second important finding of this study is the demonstration that rimonabant modulates SNS activity and energy metabolism mainly through CB_1 expressed in forebrain and sympathetic neurons. Indeed, rimonabant-induced BAT thermogenesis under cold exposure was comparable to that observed in untreated CaMK-*CB_1*-KO mice. Moreover, sympathectomy reduced BAT activity of both CaMK-*CB_1*-KO and WT mice treated with rimonabant. This last observation is in agreement with recent data showing that the effects of rimonabant on energy expenditure and thermogenesis are attenuated by BAT denervation (Verty et al., 2009).

Exposure to HFD stimulates ECS activity by enhancing endocannabinoids production (Kunos et al., 2008). Due to the inhibitory effects of CB_1 signaling, the HFD-induced activation of the ECS likely dampens neuronal pathways controlling SNS activity, leading to decreased SNS activity that, in turn, favors energy storage and fat accumulation. Conversely, in CaMK-*CB_1*-KO mice, the reduced ECS signaling at the level of forebrain and/or sympathetic neurons favors SNS overactivity, thus leading to the lean phenotype observed, particularly under HFD. Considering that HFD increases general ECS activity, a possible interpretation of our data is that, in conditions of excessive energy intake, CB_1 signaling in forebrain and/or sympathetic neurons is particularly involved in limiting SNS overactivation during DIO. Importantly, the activation of presynaptic CB_1 receptors is known to inhibit norepinephrine release and consequently reduce sympathetic "tone" onto peripheral tissues (Kunos et al., 2008); therefore, it is possible that CB_1 reduction in sympathetic ganglia is the factor leading to the increased sympathetic activation in the mutant mice. However, an alternative possibility is that central CB_1 signaling might indirectly regulate sympathetic activity through descending pathways. Further studies using mutant mice with exclusive and complete deletion of CB_1 in sympathetic ganglia will reveal the relative contribution of central nervous system versus SNS endocannabinoid signaling in the control of peripheral energy metabolism.

Finally, we have also demonstrated that deletion of CB_1 in forebrain and sympathetic neurons influences CB_1 expression in peripheral organs. CaMK-*CB_1*-KO mice, as opposed to WT mice, did not increase CB_1 expression in the BAT after HFD. This supports the existence of a "vicious ECS cycle," in which CB_1 signaling might promote itself in pathological conditions, thus contributing to the worsening of the disease.

The present findings might have an important impact on clinical practice. CB_1 receptor antagonists have been recently proposed as antiobesity agents and have been successfully tested in humans in relation to their ability to reduce body weight and improve several metabolic parameters (Scheen, 2008; Addy et al., 2008). However, their clinical use has been recently halted by the European Medicines Agency for the increased incidence of psychiatric side effects (Akbas et al., 2009) due to their action on CB_1 located in brain areas regulating mood and response to stress. Therefore, the selective targeting of peripheral CB_1 antagonists unable to cross the blood brain barrier is the next

Figure 3. Phenotype of CaMK-*CB_1*-KO Mice during High-Fat/Super High-Fat Diet

(A) CB_1 mRNA expression by QT-PCR in the white adipose tissue (WAT), brown adipose tissue (BAT), and liver of CaMK-*CB_1*-WT and CaMK-*CB_1*-KO mice fed with SD (white columns) or HFD (black columns). n = 7 per genotype and diet. AU, arbitrary units.

(B) Body weight of CaMK-*CB_1*-WT (black triangles) and CaMK-*CB_1*-KO mice (red triangles) during the 12 weeks of HFD. n = 24 per genotype. ***p < 0.0005.

(C) Body weight of *CB_1*-WT mice (n = 25) (black triangles) and complete *CB_1*-KO mice (n = 20) (gray diamonds) during the 12 weeks of HFD. ***p < 0.0005.

(D) Weight gain expressed as percentage of initial weight in CaMK-*CB_1*-KO (red triangles), complete *CB_1*-KO (gray diamonds), and their WT (black circles). **p < 0.005 CaMK-*CB_1*-KO versus WT mice; #p < 0.05 CaMK-*CB_1*-KO versus *CB_1*-KO. The values of the CaMK-*CB_1*-WT and *CB_1*-WT were cumulated, since not statistically different.

(E) Weight change expressed as percentage of initial weight in mice daily treated with rimonabant (10 mg/kg i.p.) for 32 days. (Black triangles) CaMK-*CB_1*-WT vehicle (n = 6). (Red triangles) CaMK-*CB_1*-KO vehicle (n = 5). (Blue squares) CaMK-*CB_1*-WT rimonabant (n = 7). (Green circles) CaMK-*CB_1*-KO rimonabant (n = 6). #p < 0.0005 CaMK-*CB_1*-WT rimonabant versus CaMK-*CB_1*-WT vehicle; ***p < 0.0005 CaMK-*CB_1*-WT rimonabant versus CaMK-*CB_1*-KO rimonabant.

(F) Body weight of CaMK-*CB_1*-WT (black triangles) and CaMK-*CB_1*-KO mice (red triangles) during 12 weeks of super HFD (n = 5 per genotype).

(G) Weight gain in CaMK-*CB_1*-WT and CaMK-*CB_1*-KO mice fed with mild HFD (40% of fat) (white bars) or super HFD (60% of fat) (black bars). *p < 0.05; ***p < 0.0005.

Data represent mean ± SEM.

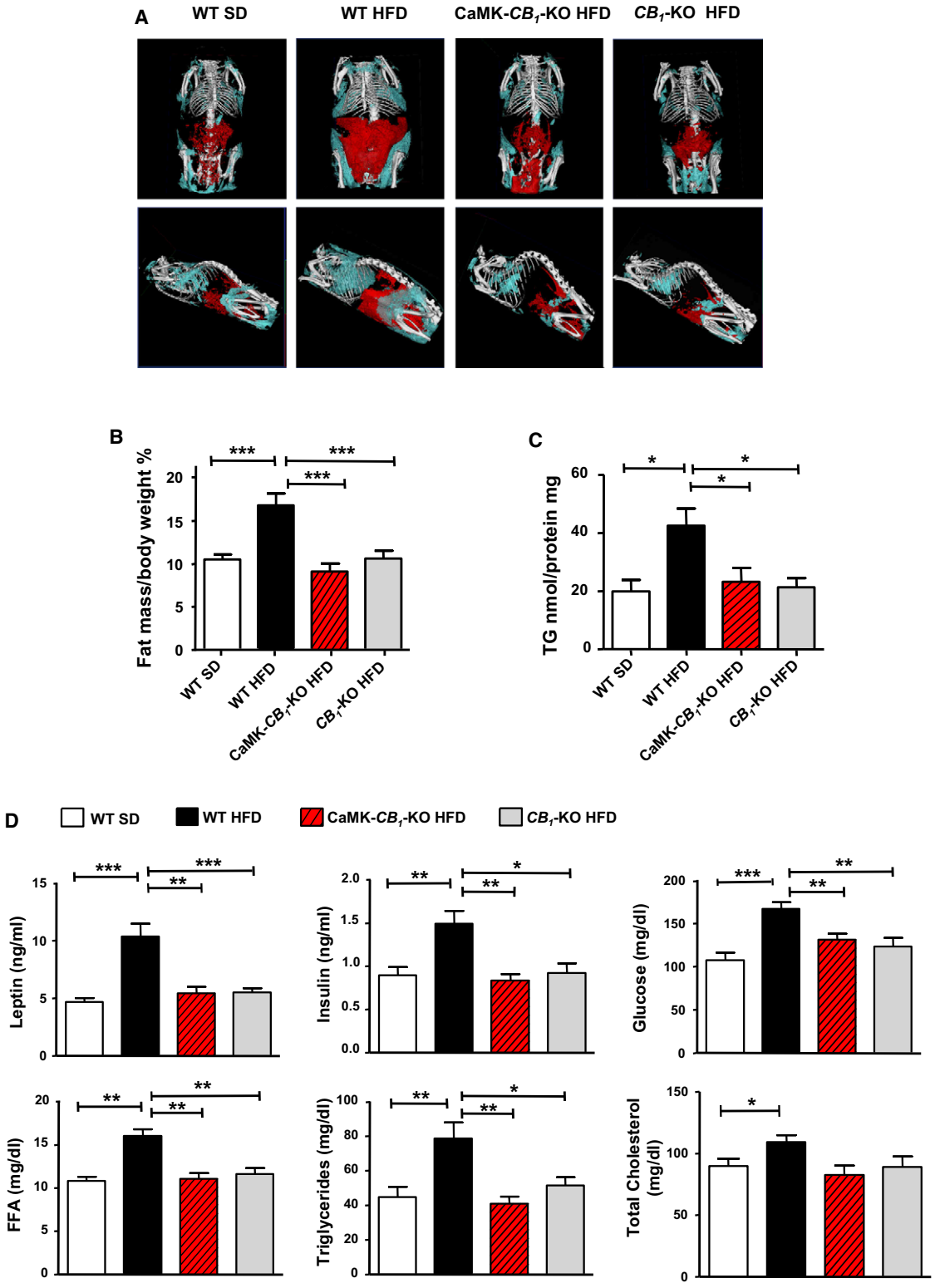

Figure 4. Characterization of CaMK-CB_1-KO Mice during High-Fat Diet

(A) Three-dimensional visualization of skeleton, visceral adipose tissue (red), and subcutaneous adipose tissue (blue) from in vivo micro-CT images of a WT on SD, WT on HFD, CaMK-CB_1-KO on HFD, and complete CB_1-KO on HFD, respectively. (Top) Frontal views. (Bottom) Lateral views.

(B) Quantification of total fat content (as percentage of body weight) by in vivo micro-CT analysis in WT mice fed on SD (white bar, n = 15), WT mice fed on HFD (black bar, n = 16), CaMK-CB_1-KO mice fed on HFD (red dashed bar, n = 11), and complete CB_1-KO mice on HFD (gray bar, n = 13). ***p < 0.0005.

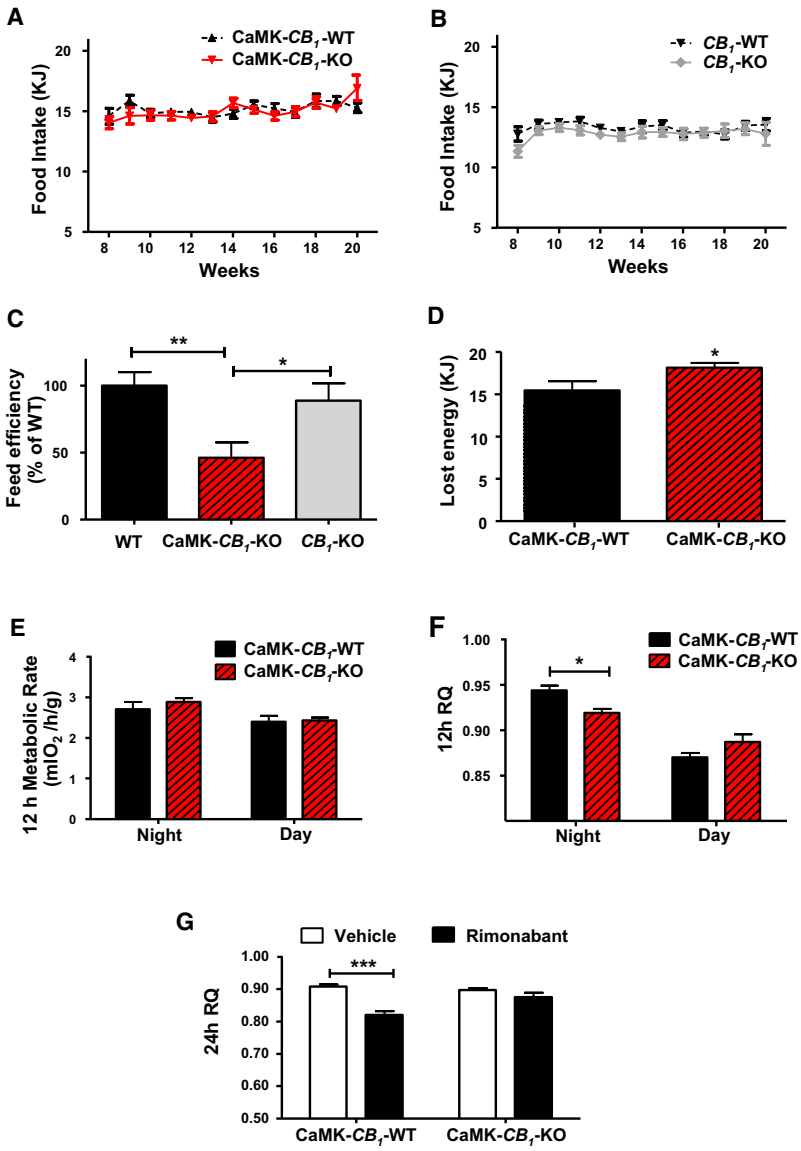

Figure 5. Energy Homeostasis in CaMK-CB_1-KO Mice on High-Fat Diet

(A) Food intake of CaMK-CB_1-WT (black triangles) and CaMK-CB_1-KO mice (red triangles) during the 12 weeks of HFD (n = 24 per genotype).

(B) Food intake of CB_1-WT (n = 25) (black triangles) and CB_1-KO mice (n = 20) (gray diamonds) during the 12 weeks of HFD.

(C) Feed efficiency of WT (black bar), CaMK-CB_1-KO (red dashed bar), and complete CB_1-KO mice (gray bar) during the 12 weeks of HFD (n = 20 per genotype). *p < 0.05; **p < 0.005. Data are expressed as percentage of WT. The values of the CaMK-CB_1-WT and CB_1-WT mice were grouped since not statistically different.

(D) Daily energy loss (24 hr energy content by bomb calorimetry). CaMK-CB_1-WT (n = 6, black bar) and CaMK-CB_1-KO (n = 7, dashed red bar) fed with HFD. *p < 0.05.

(E) Metabolic rate at night (7:00 PM–7:00 AM) and during the day (7:00 AM–7:00 PM) in CaMK-CB_1-WT (n = 5, black bar) and CaMK-CB_1-KO mice (n = 6, dashed red bar) on HFD.

(F) Average RQ at night (7:00 PM–7:00 AM) and during the day (7:00 AM–7:00 PM) in CaMK-CB_1-WT (n = 5, black bar) and CaMK-CB_1-KO mice (n = 6, dashed red bar) on HFD. *p < 0.05.

(G) Average RQ measured every hour for two days in CaMK-CB_1-WT (n = 7) and CaMK-CB_1-KO (n = 6) fed with HFD. On the first day, animals were treated with vehicle; rimonabant treatment (10 mg/kg i.p.) started at the beginning of day 2. ***p < 0.0005. White bars, vehicle-treated mice; black bars, rimonabant-treated mice.

Data represent mean ± SEM.

predictable step in order to minimize side effects and, at the same time, retain the favorable metabolic actions due to CB_1 inhibition at the level of the adipose tissue, liver, skeletal muscle, and endocrine pancreas (Kunos et al., 2009). Our results point to a key role of CB_1 expressed in forebrain neurons and sympathetic terminals in the control of energy metabolism but leave open the possibility that nonblood brain barrier-penetrating drugs (McElroy et al., 2008; LoVerme et al., 2009), acting at presynaptic CB_1 receptors on peripheral neurons and thereby on nonneuronal peripheral organs, may importantly contribute to reduce the negative effect of the overactivation of the ECS described in association with obesity and related disorders.

EXPERIMENTAL PROCEDURES

Animals

Male CB_1-KO mice, CaMK-CB_1-KO mice (CB_1 receptor deletion in neurons expressing the Ca^{2+}/calmodulin-dependent kinase IIα), and their WT littermates were genotyped as described (Marsicano et al., 2002; Monory et al., 2006). Mutant animals were in a mixed genetic background, with a predominant C57BL/6N contribution (seven backcrosses). Mice were housed in individual cages under conditions of controlled temperature (24°C) and illumination (12 hr light/12 hr dark cycle) in the DIMORFIPA animal facilities, University of Bologna, Italy. All of the procedures were approved by the Central Veterinary Office of Bologna University in accordance with the European Community (86/609/EEC) guidelines for the care and use of laboratory animals. Animals were fed either with a mouse SD containing 12.3 KJ/g (11% fat, 19% protein, 70% carbohydrate; Dr. Piccioni Lab, Gessate, Milano, Italy), with an HFD having 18.9 KJ/g (40% fat, 15% protein, 45% carbohydrate; Dottor Piccioni Lab), or with a super HFD (SHFD) having 21.3 KJ/g (60.3% fat, 18.4% protein, 21.3% carbohydrate; TD.06414 Harlan Teklad, Italy). Eight-week-old mice were placed on HFD or SHFD or were maintained on SD. Body weight was measured twice a week starting at 8 weeks until 20 weeks of age (when not mentioned otherwise).

(C) Hepatic triglycerides (TG) content in WT mice fed with SD (white bar, n = 7), WT on HFD (black bar, n = 6), CaMK-CB_1-KO on HFD (red dashed bar, n = 8), and CB_1-KO on HFD (gray bar, n = 8). *p < 0.05.

(D) Hormonal profile in WT mice fed with SD (white bar), WT on HFD (black bar), CaMK-CB_1-KO on HFD (red dashed bar), CB_1-KO on HFD (gray bar). Leptin, insulin, and FFA: n = 20 per genotype and diet. Triglycerides and total cholesterol: n = 12. Glucose: n = 12. ***p < 0.0005; **p < 0.005; *p < 0.05.

Data in (B)–(D) represent mean ± SEM. The values of the CaMK-CB_1-WT and CB_1-WT in SD or HFD were cumulated in (B) and (C) since not statistically different.

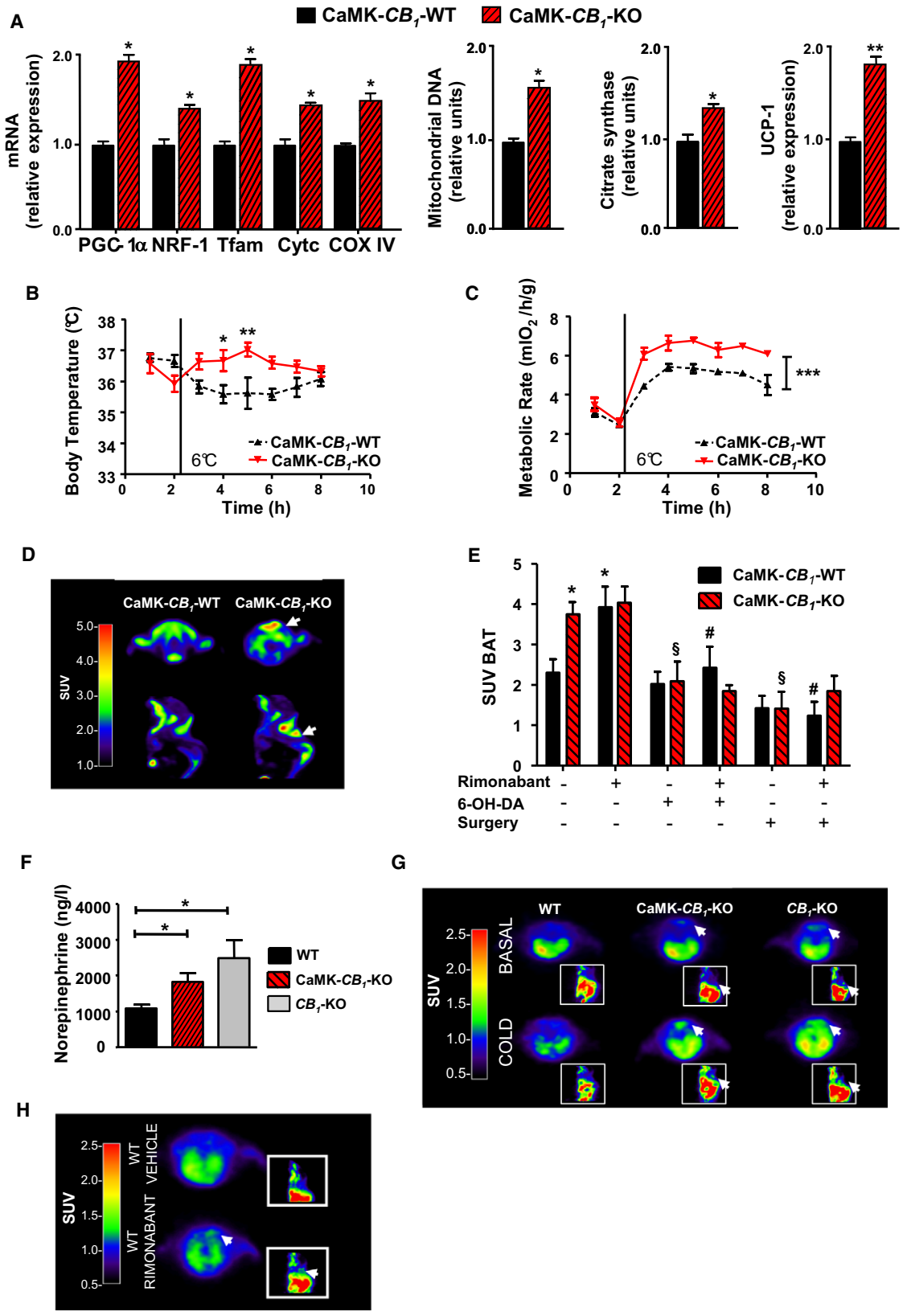
A
CaMK-CB1-WT
CaMK-CB1-KO
mRNA (relative expression)
PGC-1α
NRF-1
Tfam
Cytc
COX IV
Mitochondrial DNA (relative units)
Citrate synthase (relative units)
UCP-1 (relative expression)
B
Body Temperature (℃)
Time (h)
6℃
C
Metabolic Rate (mlO2/h/g)
D
SUV
E
SUV BAT
Rimonabant
6-OH-DA
Surgery
F
Norepinephrine (ng/l)
WT
CaMK-CB1-KO
CB1-KO
G
BASAL
COLD
H
VEHICLE
RIMONABANT

In Situ Hybridization

All tissues were derived from mice on SD. In situ hybridization (ISH) and DISH were performed using a radioactive or a nonradioactive (dig-labeled) CB_1-specific riboprobe and a nonradioactive (dig-labeled) GLP-1 in the hypothalamus, NTS, and nodose ganglia or a dopamine β-hydroxylase (DBH)-specific riboprobe in superior cervical sympathetic ganglia (Marsicano and Lutz, 1999) (see Supplemental Information).

IHC and Immunofluorescence

Polyclonal goat antibody (ab) (1:900) against the C-terminal 31 amino acids (443–473) of mouse CB_1 was used to stain hypothalamus and brainstem (Fukudome et al., 2004), and a polyclonal rabbit antiserum (1:300) against the last 73 amino acid residues of rat CB_1 (Wager-Miller et al., 2002) was used to stain nodose ganglion (generous gift of Dr. K. Mackie, Indiana University, Bloomington, IN). The specificity of the CB_1 antibodies was described elsewhere (Makara et al., 2007; Wager-Miller et al., 2002). Anti-tyrosine hydroxylase rabbit polyclonal ab (1:2000; Chemicon-Millipore, Temecula, CA 92590) detecting adrenergic nerve fibers was used in BAT. Biotinylated donkey anti-goat IgG (1:500; Jackson Lab, West Grove, PA) for hypothalamus and brainstem and rhodamine (TRITC)-conjugated affine pure donkey anti-rabbit IgG (1:200 Jackson ImmunoResearch) for BAT were used as secondary abs. For double-labeling immunofluorescence of nodose ganglia, a goat polyclonal anti-HuC/D (a panneuronal marker) (Santa Cruz Biotechnology, Inc. CA 95060) was used. As secondary abs, donkey anti-mouse IgG conjugated to fluorescein isothiocyanate (FITC) and rhodamine (TRITC)-conjugated (Jackson ImmunoResearch) (both at 1:500) were used (see Supplemental Information).

RNA Isolation and Real-Time PCR Analysis

RNA was isolated from tissues on SD or HFD (when indicated) mice and was analyzed as described (Tedesco et al., 2008) (see Supplemental Information). Primer sequences are in Table S1.

Immunoblot Analysis

The following antibodies were used: anti-PGC-1α (1: 1000, Cell Signaling), anti-COX IV (1:500, Molecular Probes), anti-Cyt c (1:500, BD Bioscience), anti-UCP-1 (1:1000, Calbiochem), and anti-GAPDH (1:20000 Histo-Line Laboratories) (see Supplemental Information).

Food Intake and Feed Efficiency

Food intake of mice allowed to food and water ad libitum was measured twice a week starting at 8 weeks until 20 weeks of age. Feed efficiency was calculated over the 12 weeks of diet as body weight gained per unit of energy intake (g/KJ). For the other studies on food intake, see Supplemental Information.

Hormone and Metabolite Assays

Plasma leptin was measured by Mouse Leptin RIA kit ML-82k (Millipore Corporation), insulin by Rat Insulin RIA kit RI-13K (Millipore Corporation), FFA by a colorimetric method (Wako Chemicals, Richmond, VA), triglycerides and total cholesterol by spectrophotometric enzymatic test (Roche Diagnostics, Mannheim, Germany), and glucose by the Breeze glucometer (Bayer). Plasma catecholamines were determined by high-performance liquid chromatography (Grossi et al., 1991). Blood for cathecolamines determination was obtained from nonanesthetized animals via surgically implanted intracardiac catheters. Haepatic lipids were extracted in chloroform/methanol 2:1 (0.01% BHT) and analyzed by BV-K622-100 kit (BoVision, Mountain View, CA).

In Vivo Quantification of Adipose Tissue

Mice were placed under anesthesia with 5% sevoflurane and oxygen supplementation (1 l/min) and scanned in an in vivo microcomputed tomography (micro-CT) scanner (eXplore Locus, GE, Milwaukee) at an isometric resolution of 90 μm (see Supplemental Information).

Energy Expenditure

Animals were kept individually in type II Makrolon cages inside a climate chamber. RQ and metabolic rate data were collected every hour in animals with free access to food and water. Some experiments were performed in two consecutive days. On day 1, mice were studied in their physiological conditions at ambient temperature. At the beginning of the light phase of day 2, mice were treated with rimonabant (10 mg/kg i.p.). Experiments under cold conditions were performed with an initial period of acclimation of the mice in the chambers (at 24°C for 3 hr), followed by a lowering of chambers temperature to 6°C (see Supplemental Information).

Telemetric Recording of Body Temperature

Animals were i.p. implanted with calibrated temperature transmitters (Mini-Mitter, Model X, Sunriver, Oregon, accuracy 0.1°C) under ketamine-hydrochloride anesthesia (50 $mg*kg^{-1}$) and 1%–2% isoflurane. The detection of the transmitter signals was accomplished by a radio receiver and processed by a microcomputer system.

Food and Feces Energy Content

Energy content of food and energy loss via the feces were determined using bomb calorimetry (IKA-Calorimeter C 5000, IKA-Werke GmbH & Co. KG, Staufen, Germany).

Mitochondrial DNA Analysis and Citrate Synthase Activity

Mitochondrial DNA analysis was performed and citrate synthase activity was measured as described in Tedesco et al., 2008.

Figure 6. Increased Thermogenesis and Sympathetic Tone in CaMK-CB_1-KO on High-Fat Diet

(A) Mitochondrial biogenesis and UCP1 mRNA levels in BAT of CaMK-CB_1-WT (black bars) and CaMK-CB_1-KO mice (dashed red bars) fed with HFD. PGC-1α, NRF-1, Tfam, COX IV, Cyt c mRNA level, and mitochondrial DNA amounts were analyzed by QT-PCR. CaMK-CB_1-WT: n = 7; CaMK-CB_1-KO: n = 8. **p < 0.005 versus CaMK-CB_1-WT mice.

(B) Body temperature in CaMK-CB_1-WT (black triangles) (n = 5) and CaMK-CB_1-KO mice (red triangles) (n = 6) on HFD during 6 hr of cold exposure (+6°C). *p < 0.05; **p < 0.005.

(C) Metabolic rate in CaMK-CB_1-WT (black triangles) (n = 5) and CaMK-CB_1-KO mice (red triangles) (n = 6) on HFD during 6 hr at +6°C. ***p < 0.0005.

(D) Representative PET image showing ^{18}F-FDG accumulation in the soprascapular BAT (arrows) of a CaMK-CB_1-WT and CaMK-CB_1-KO mouse at +6°C. (Top) Axial section. (Bottom) Sagittal section.

(E) Quantification of ^{18}F-FDG uptake (SUV) in the soprascapular BAT of CaMK-CB_1-WT (black bar) and CaMK-CB_1-KO mice (dashed red bar) under HFD after cold exposure and different treatments. The cohorts were composed of mice treated with: vehicle (n = 12 WT, n = 9 KO), vehicle + 6-0H-DA (n = 6 WT, n = 6 KO), vehicle + surgically denervation (n = 6 WT, n = 6 KO). For each cohort, the analysis was repeated on the same mice after rimonabant treatment. *p < 0.05 versus CaMK-CB_1-WT vehicle; §p < 0.05 versus CaMK-CB_1-KO vehicle; #p < 0.05 versus CaMK-CB_1-WT rimonabant.

(F) Plasma norepinephrine levels in WT (black bar, n = 12), CaMK-CB_1-KO (dashed red bars, n = 7), and CB_1-KO mice (gray bar, n = 9) on HFD. *p < 0.05 versus WT. The values of the CaMK-CB_1-WT and CB_1-WT mice were grouped since not statistically different.

(G) Representative PET image showing the uptake of ^{11}C-meta-hydroxyephedrine in the BAT (arrow) of WT (n = 4), CaMK-CB_1-KO (n = 4), and CB_1-KO (n = 3) mice in basal state and after cold exposure.

(H) Representative PET image showing ^{11}C-meta-hydroxyephedrine uptake (at 24°C) in the BAT (arrow) of WT mice chronically treated with vehicle or rimonabant (10 mg/kg) for 32 days.

Radioactive counts in (D), (G), and (H) are expressed as standard uptake values (SUV); smaller insets in (G) and (H) represent sagittal view. Data in (A–C), (E), and (F) represent mean ± SEM. See also Figure S2.

Small Animal PET Studies

For ^{18}F-FDG studies, 20-week-old mice were imaged in two different sessions. In the first, 8 hr fasted mice were placed at 24°C and i.p. treated with a vehicle solution; 1 hr later, mice were moved to a cold chamber (6°C) for 3 hr. Mice were then lightly anesthetized (gas sevofluorane), injected with ^{18}F-FDG (15 MBq), allowed to awake, and placed in a cold chamber for 1 hr (phase of tracer uptake). Scans were performed with a PET system (Explore Vista, GE) in animals treated with vehicle (3% DMSO, 1% Tween80 in saline solution) or vehicle + sympathetic denervation and repeated after 5 days of stabilization in the same animals treated with rimonabant (10 mg/kg i.p.). Control mice after sympathectomy (vehicle of 6-hydroxydopamine hydrobromide [6-OH-DA] and sham-operated mice) did not present different values of FDG uptake compared to WT mice treated with the vehicle of rimonabant (data not shown); thus, they were not included in the analysis.

For ^{11}C-meta-hydroxyephedrine studies, PET scan started immediately after the tracer injection (20 MBq) in the tail vein of anaesthetized animals. Imaging was first performed on 20-week-old animals at 24°C and then repeated (after 5 days) in the same animals exposed to cold (6°C) for 3 hr. Data for accumulation of ^{18}F-FDG and ^{11}C-meta-hydroxyephedrine on small animal PET images were expressed as standard uptake values (SUV) representing radioactive counts per gram of tissue, divided by injected dose of radioactivity per gram of animal weight. To correctly identify BAT uptake of the tracers, a CT reference image was coregistered with the PET image for each scan as described in Galiè et al., 2007.

Sympathectomy

For the chemical sympathectomy, mice were i.p. treated with injections of 80 mg/kg of 6-OH-DA in 0.1% ascorbic acid or vehicle daily for 3 consecutive days. Surgical sympathectomy of BAT was performed by cutting each of the nerve bundles projecting into the left and the right soprascapular pads. For the sham-operated animals, the BAT and the nerves were exposed, but not transected. Animals were allowed to recover for 10 days before testing. For histological verification of denervation, see Figure S2C.

Statistics

Results are expressed as mean ± SEM. Statistical analysis was performed by unpaired two-tailed Student's t test or by analysis of variance (ANOVA) with appropriate posthoc tests. The software GraphPad Prism 5.0 was used. A p value less than 0.05 was considered statistically significant.

SUPPLEMENTAL INFORMATION

Supplemental Information includes Supplemental Experimental Procedures, two figures, and one table and can be found with this article online at doi:10.1016/j.cmet.2010.02.015.

ACKNOWLEDGMENTS

This research was supported by grants from: European Union (LSHM-CT-2003-503041 to U.P.), European Union REPROBESITY (FPVII-223713 to U.P., G. Marsicano, and B. Lutz); 2007 PRIN from MIUR (to U.P. and E.N.); FIRB 2003 RBNE03KZRJ_002 (to R.P.); Avenir Program of INSERM (to D.C. and G. Marsicano); in part by the DFG (to B. Lutz); the European Foundation for the Studies of Diabetes (EFSD) (to G. Marsicano, B. Lutz, and D.C.), Fondation Bettencourt Schueller (to G. Marsicano); Bourse Ministerielle de Doctorat (to L. Bellocchio); Fondazione Cassa di Risparmio Bologna (to R.D.G.). We acknowledge Dr. K. Mackie (The Linda and Jack Gill Center for Biomolecular Science, Indiana University, Bloomington, IN) for the gift of polyclonal rabbit CB_1 antiserum and Dr. S. Boschi (Radiopharmacy, Department of Nuclear Medicine, S. Orsola-Malpighi Hospital, University of Bologna, Italy) for the synthesis of PET tracers.

Received: July 10, 2009
Revised: December 22, 2009
Accepted: February 26, 2010
Published: April 6, 2010

REFERENCES

Addy, C., Wright, H., Van Laere, K., Gantz, I., Erondu, N., Musser, B.J., Lu, K., Yuan, J., Sanabria-Bohórquez, S.M., Stoch, A., et al. (2008). The acyclic CB1R inverse agonist taranabant mediates weight loss by increasing energy expenditure and decreasing caloric intake. Cell Metab. *7*, 68–78.

Akbas, F., Gasteyger, C., Sjödin, A., Astrup, A., and Larsen, T.M. (2009). A critical review of the cannabinoid receptor as a drug target for obesity management. Obes. Rev. *10*, 58–67.

Casanova, E., Fehsenfeld, S., Mantamadiotis, T., Lemberger, T., Greiner, E., Stewart, A.F., and Schütz, G. (2001). A CamKIIalpha iCre BAC allows brain-specific gene inactivation. Genesis *31*, 37–42.

Cota, D., Marsicano, G., Tschöp, M., Grübler, Y., Flachskamm, C., Schubert, M., Auer, D., Yassouridis, A., Thöne-Reineke, C., Ortmann, S., et al. (2003). The endogenous cannabinoid system affects energy balance via central orexigenic drive and peripheral lipogenesis. J. Clin. Invest. *112*, 423–431.

Cota, D., Sandoval, D.A., Olivieri, M., Prodi, E., D'Alessio, D.A., Woods, S.C., Seeley, R.J., and Obici, S. (2009). Food intake-independent effects of CB1 antagonism on glucose and lipid metabolism. Obesity (Silver Spring) *17*, 1641–1645.

Di Marzo, V., Goparaju, S.K., Wang, L., Liu, J., Bátkai, S., Járai, Z., Fezza, F., Miura, G.I., Palmiter, R.D., Sugiura, T., and Kunos, G. (2001). Leptin-regulated endocannabinoids are involved in maintaining food intake. Nature *410*, 822–825.

Fukudome, Y., Ohno-Shosaku, T., Matsui, M., Omori, Y., Fukaya, M., Tsubokawa, H., Taketo, M.M., Watanabe, M., Manabe, T., and Kano, M. (2004). Two distinct classes of muscarinic action on hippocampal inhibitory synapses: M2-mediated direct suppression and M1/M3-mediated indirect suppression through endocannabinoid signalling. Eur. J. Neurosci. *19*, 2682–2692.

Galiè, M., Farace, P., Nanni, C., Spinelli, A., Nicolato, E., Boschi, F., Magnani, P., Trespidi, S., Ambrosini, V., Fanti, S., et al. (2007). Epithelial and mesenchymal tumor compartments exhibit in vivo complementary patterns of vascular perfusion and glucose metabolism. Neoplasia *9*, 900–908.

Grill, H.J., and Hayes, M.R. (2009). The nucleus tractus solitarius: a portal for visceral afferent signal processing, energy status assessment and integration of their combined effects on food intake. Int. J. Obes. (Lond.) *33* (*Suppl 1*), S11–S15.

Grossi, G., Bargossi, A.M., Lucarelli, C., Paradisi, R., Sprovieri, C., and Sprovieri, G. (1991). Improvements in automated analysis of catecholamine and related metabolites in biological samples by column-switching high-performance liquid chromatography. J. Chromatogr. *22*, 273–284.

Herling, A.W., Kilp, S., Elvert, R., Haschke, G., and Kramer, W. (2008). Increased energy expenditure contributes more to the body weight-reducing effect of rimonabant than reduced food intake in candy-fed wistar rats. Endocrinology *149*, 2557–2566.

Jbilo, O., Ravinet-Trillou, C., Arnone, M., Buisson, I., Bribes, E., Péleraux, A., Pénarier, G., Soubrié, P., Le Fur, G., Galiègue, S., and Casellas, P. (2005). The CB1 receptor antagonist rimonabant reverses the diet-induced obesity phenotype through the regulation of lipolysis and energy balance. FASEB J. *19*, 1567–1569.

Kunos, G., Osei-Hyiaman, D., Liu, J., Godlewski, G., and Bátkai, S. (2008). Endocannabinoids and the control of energy homeostasis. J. Biol. Chem. *283*, 33021–33025.

Kunos, G., Osei-Hyiaman, D., Bátkai, S., Sharkey, K.A., and Makriyannis, A. (2009). Should peripheral CB(1) cannabinoid receptors be selectively targeted for therapeutic gain? Trends Pharmacol. Sci. *30*, 1–7.

LoVerme, J., Duranti, A., Tontini, A., Spadoni, G., Mor, M., Rivara, S., Stella, N., Xu, C., Tarzia, G., and Piomelli, D. (2009). Synthesis and characterization of a peripherally restricted CB1 cannabinoid antagonist, URB447, that reduces feeding and body-weight gain in mice. Bioorg. Med. Chem. Lett. *19*, 639–643.

Makara, J.K., Katona, I., Nyíri, G., Németh, B., Ledent, C., Watanabe, M., de Vente, J., Freund, T.F., and Hájos, N. (2007). Involvement of nitric oxide in depolarization-induced suppression of inhibition in hippocampal pyramidal cells during activation of cholinergic receptors. J. Neurosci. *27*, 10211–10222.

Marsicano, G., and Lutz, B. (1999). Expression of the cannabinoid receptor CB1 in distinct neuronal subpopulations in the adult mouse forebrain. Eur. J. Neurosci. *11*, 4213–4225.

Marsicano, G., Wotjak, C.T., Azad, S.C., Bisogno, T., Rammes, G., Cascio, M.G., Hermann, H., Tang, J., Hofmann, C., Zieglgänsberger, W., et al. (2002). The endogenous cannabinoid system controls extinction of aversive memories. Nature *418*, 530–534.

Marsicano, G., Goodenough, S., Monory, K., Hermann, H., Eder, M., Cannich, A., Azad, S.C., Cascio, M.G., Gutiérrez, S.O., van der Stelt, M., et al. (2003). CB1 cannabinoid receptors and on-demand defense against excitotoxicity. Science *302*, 84–88.

McElroy, J., Sieracki, C., and Chorvat, R. (2008). Non-brain penetrant CB1 receptor antagonists as novel treatment of obesity and related metabolic disorders. Obesity (Silver Spring) *16* (*Suppl. 1*), S47.

Monory, K., Massa, F., Egertová, M., Eder, M., Blaudzun, H., Westenbroek, R., Kelsch, W., Jacob, W., Marsch, R., Ekker, M., et al. (2006). The endocannabinoid system controls key epileptogenic circuits in the hippocampus. Neuron *51*, 455–466.

Nogueiras, R., Veyrat-Durebex, C., Suchanek, P.M., Klein, M., Tschöp, J., Caldwell, C., Woods, S.C., Wittmann, G., Watanabe, M., Liposits, Z., et al. (2008). Peripheral, but not central, CB1 antagonism provides food intake-independent metabolic benefits in diet-induced obese rats. Diabetes *57*, 2977–2991.

Osei-Hyiaman, D., Liu, J., Zhou, L., Godlewski, G., Harvey-White, J., Jeong, W.I., Bátkai, S., Marsicano, G., Lutz, B., Buettner, C., and Kunos, G. (2008). Hepatic CB1 receptor is required for development of diet-induced steatosis, dyslipidemia, and insulin and leptin resistance in mice. J. Clin. Invest. *118*, 3160–3169.

Pagotto, U., Marsicano, G., Cota, D., Lutz, B., and Pasquali, R. (2006). The emerging role of the endocannabinoid system in endocrine regulation and energy balance. Endocr. Rev. *27*, 73–100.

Ravinet Trillou, C., Delgorge, C., Menet, C., Arnone, M., and Soubrié, P. (2004). CB1 cannabinoid receptor knockout in mice leads to leanness, resistance to diet-induced obesity and enhanced leptin sensitivity. Int. J. Obes. Relat. Metab. Disord. *28*, 640–648.

Scheen, A.J. (2008). CB1 receptor blockade and its impact on cardiometabolic risk factors: overview of the RIO programme with rimonabant. J. Neuroendocrinol. *20* (*Suppl 1*), 139–146.

Tedesco, L., Valerio, A., Cervino, C., Cardile, A., Pagano, C., Vettor, R., Pasquali, R., Carruba, M.O., Marsicano, G., Lutz, B., et al. (2008). Cannabinoid type 1 receptor blockade promotes mitochondrial biogenesis through endothelial nitric oxide synthase expression in white adipocytes. Diabetes *57*, 2028–2036.

Thackeray, J.T., Beanlands, R.S., and Dasilva, J.N. (2007). Presence of specific 11C-meta-Hydroxyephedrine retention in heart, lung, pancreas, and brown adipose tissue. J. Nucl. Med. *48*, 1733–1740.

Tsou, K., Brown, S., Sañudo-Peña, M.C., Mackie, K., and Walker, J.M. (1998). Immunohistochemical distribution of cannabinoid CB1 receptors in the rat central nervous system. Neuroscience *83*, 393–411.

Verty, A.N., Allen, A.M., and Oldfield, B.J. (2009). The effects of rimonabant on brown adipose tissue in rat: implications for energy expenditure. Obesity (Silver Spring) *17*, 254–261.

Wager-Miller, J., Westenbroek, R., and Mackie, K. (2002). Dimerization of G protein-coupled receptors: CB1 cannabinoid receptors as an example. Chem. Phys. Lipids *121*, 83–89.

Wittmann, G., Deli, L., Kalló, I., Hrabovszky, E., Watanabe, M., Liposits, Z., and Fekete, C. (2007). Distribution of type 1 cannabinoid receptor (CB1)-immunoreactive axons in the mouse hypothalamus. J. Comp. Neurol. *503*, 270–279.